A Fuzzy-Bayesian belief network model for coastal flood vulnerability assessment

Valentina Velandia-Diaz, Emilio Bastidas-Arteaga, Axel Creach, Solomon Tesfamariam

Progress in Disaster Science 30 (2026) 100583

Contents lists available at ScienceDirect

Progress in Disaster Science

journal homepage: www.elsevier.com/locate/pdisas

Regular Article

A Fuzzy-Bayesian belief network model for coastal flood vulnerability assessment

Valentina Velandia-Diaz [a], Emilio Bastidas-Arteaga [a,*], Axel Creach [b], Solomon Tesfamariam [c]

[a] La Rochelle Université, Laboratoire des Sciences de l'Ingénieur pour l'Environnement, LaSIE, Avenue Michel Crépeau, La Rochelle, 17042, France
[b] Université de Brest, Nantes Université, Université de Rennes, LETG, UMR 6554, F-29280, Plouzané, France
[c] University of Waterloo, Department of Civil and Environmental Engineering, 200 University Avenue West, Waterloo, N2L 3G1, Ontario, Canada

ARTICLE INFO

Keywords:
Coastal flooding
Flood vulnerability index
Fuzzy Bayesian belief network
Uncertainty propagation
Residential houses
Climate change

ABSTRACT

Flood risk poses a significant threat to coastal areas, with climate change and urbanization intensifying the frequency and severity of flood events. Effective flood risk management requires quantifying vulnerability while accounting for the inherent uncertainty in residential areas exposed to coastal hazards. This study revisits the flood vulnerability index (VIE), which evaluates life loss risk in residential buildings using four microscale criteria, and enhances it with a fuzzy Bayesian belief network (FBBN). The FBBN framework integrates uncertainty and conditional dependencies into the assessment by fuzzifying input criteria and estimating the probability of buildings belonging to various vulnerability classes. The proposed framework was applied to a case study on the island of Noirmoutier (France), evaluating the vulnerability of 21,046 buildings across four flooding scenarios. The FBBN demonstrated good consistency with the original deterministic VIE index, with less than 3% outliers in classification results. Sensitivity analysis identified architectural typology as the most influential criterion, contributing 10%–11% variance reduction across all scenarios. The FBBN provided probabilistic and geo-spatial representations of vulnerability, offering a deeper understanding of risk distribution. These insights enhance decision-making in flood adaptation planning, supporting more targeted and effective mitigation strategies.

1. Introduction

Coastal flood risk is projected to increase significantly in the coming decades due to the combination of climatic factors such as sea level rise, the intensification of extreme weather events, socioeconomic drivers, urban expansion and aging infrastructure [1–3]. This trend is particularly concerning given that floods are among the most devastating and recurrent natural hazards, responsible for significant loss of life and massive economic impact worldwide [4–6]. Storm Xynthia, which struck in February 2010, serves as a tragic example of the devastating impacts of coastal flooding in Europe. The storm caused over 40 fatalities in France, with the most severe consequences observed in the Vendée and Charente-Maritime departments (Fig. 1), where strong winds combined with an unusually high tide coefficient led to a storm surge of approximately 1.5 m [7]. This surge inundated 50,000 hectares of low-lying coastal land and resulted in an estimated €1.5 billion in damages [8–10]. The event exposed critical vulnerabilities in coastal residential areas and highlighted the urgent need for more robust risk assessment frameworks to address increasing coastal flood hazards under a changing climate.

A wide range of vulnerability assessment tools and methodologies have been developed to assess and manage flood risk for various types of flooding (e.g., flash, river, coastal (as the present research)). Some approaches assess vulnerability through indices and integrate hazard mapping [12–15], hydrodynamic simulations [16,17], probabilistic methods [18–20] and machine learning [21]. A growing body of research also highlights the critical role of interdependent infrastructure networks and cascading failures in shaping flood impacts [22]. However, these studies differ notably in scope, scale and variables integrated. At a large-scale, studies typically explore broad dimensions like the physical, social, economic and environmental aspects through a series of vulnerability indicators. For instance, Kaur et al. [23] proposed a 'Localized Flood Vulnerability Index' combining a multi-criteria decision-making process, a fuzzy analytical hierarchical process and expert elicitation. Similarly, Borden et al. [24] proposed a deterministic framework to assess vulnerability through separate indices:

* Corresponding author.
E-mail address: ebastida@univ-lr.fr (E. Bastidas-Arteaga).

https://doi.org/10.1016/j.pdisas.2026.100583
Received 12 September 2025; Received in revised form 17 April 2026; Accepted 24 April 2026
Available online 5 May 2026

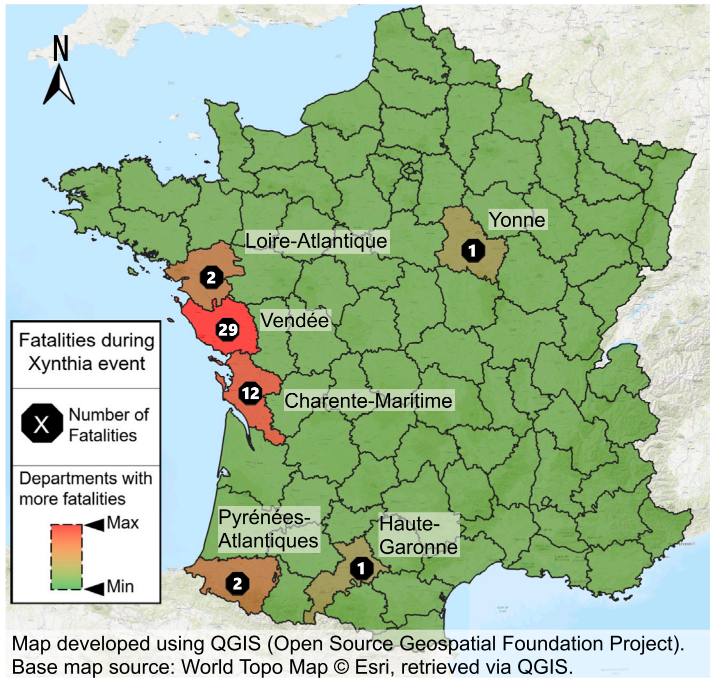

Fig. 1. Most affected departments after Xynthia event in terms of fatalities.
Source: Adapted from [11]

'Social Vulnerability Index', the 'Built Environmental Vulnerability Index' and 'Hazard Vulnerability Index'. At the mid-scale, the approaches frequently adopt the classical formulation of risk as a product of hazard, vulnerability and exposure [25]. Lu et al. [18], for example, combined Bayesian networks and GIS, in a probabilistic framework that models these three dimensions using a variety of specific indicators. Likewise, Banan et al. [19] developed a Bayesian network model to assess coastal flood risk by incorporating hazards, vulnerable receptors (such as people and roads), and associated damages. Other frameworks may focus specifically on modeling a single component; for instance, Wu et al. [26] modeled hazard using a belief network considering the drivers, bearers, and environmental factors to assess the extent of a flood disaster.

Given the complexity of flood risk assessment, with its many interacting parameters and variables, a microscale assessment of flood risk becomes a difficult task. Tincu et al. [27] evaluated damage across three land use classes (residential building, infrastructure and agriculture) using a semi-probabilistic approach that incorporates existing damage. Similarly, Rehan et al. [28] focused on the economic impact of flooding for multiple flood scenarios, assessing household level by evaluating individual residential buildings exposed to riverine flooding. Other relevant micro-scale examples include the work of Ernst et al. [29] that conducted a household-level analysis using a detailed 2D river hydraulic modeling and topographical data to predict inundation patterns with high spatial accuracy in urban floodplains. De-Risi [30] introduced the VISK (Visual Vulnerability & Risk) a computer-based flood risk module that assesses individual houses using a probabilistic framework. It employs structural fragility functions and Monte Carlo simulations within a bi-dimensional finite element model to analyze structural configurations (including openings like doors and windows) and calculate risk of failure under hydrostatic pressure, hydrodynamic forces, debris impact, and structural deterioration. The output is a GIS-based risk map that spatially defines the risk associated with each assessed building.

Although previous studies address residential buildings to some extent, most fail to adequately consider micro-scale factors that directly influence human vulnerability at the household level. Existing approaches often account for building characteristics in a binary manner (i.e., the building either resists or is destroyed) [31]. This limitation stems largely from findings in post-event analyses of flood-related mortality, which indicate that fatalities inside buildings are relatively low (6%, as reported by Jonkman and Kelman, 2005 [32]). However, the Xynthia case highlighted that the location and configuration of residential buildings can significantly increase risk, as 100% of the fatalities occurred inside houses due to their specific localization and/or configuration [7].

Furthermore, in 2019, 1.5 million people in France lived in coastal flood-prone areas, encompassing 1.3 million housing units. Among these, single-story constructions accounted for 26%–30% of buildings along the French Atlantic coast [33]. These statistics underscore the urgency of focusing flood risk assessments at the building scale, where meaningful and targeted interventions can be implemented. Additionally, a persistent limitation of existing micro-scale approaches is their restricted ability to explicitly represent uncertainty and the interdependencies between risk components [34]. This is particularly critical in complex residential environments, where effective decision-making requires adaptability and a nuanced understanding of vulnerability factors.

The current study aims to address this gap by conducting a microscale assessment focused on vulnerability and exposure, particularly in relation to residential buildings. Unlike previous studies that focus on construction materials or structural integrity, this research does not consider structural engineering features. Instead, it focuses on geographical and architectural aspects, including the architectural configuration of buildings, their elevation, and their proximity to flood defense structures and designated rescue points. These characteristics are crucial for ensuring safe evacuation in the event of an emergency.

The Extreme Intrinsic Vulnerability Index (VIE Index, *Vulnérabilité Intrinsèque Extrême* in French), developed by Creach et al. [35] following the Storm Xynthia event, represents a valuable advancement in micro-scale vulnerability assessment. This framework has also been applied to compare the effectiveness of different flood adaptation strategies [36,37]. However, the original formulation of the VIE Index is inherently deterministic. The values assigned to each vulnerability criterion are based on predefined crisp categories, which do not account for the uncertainties present in real-world events.

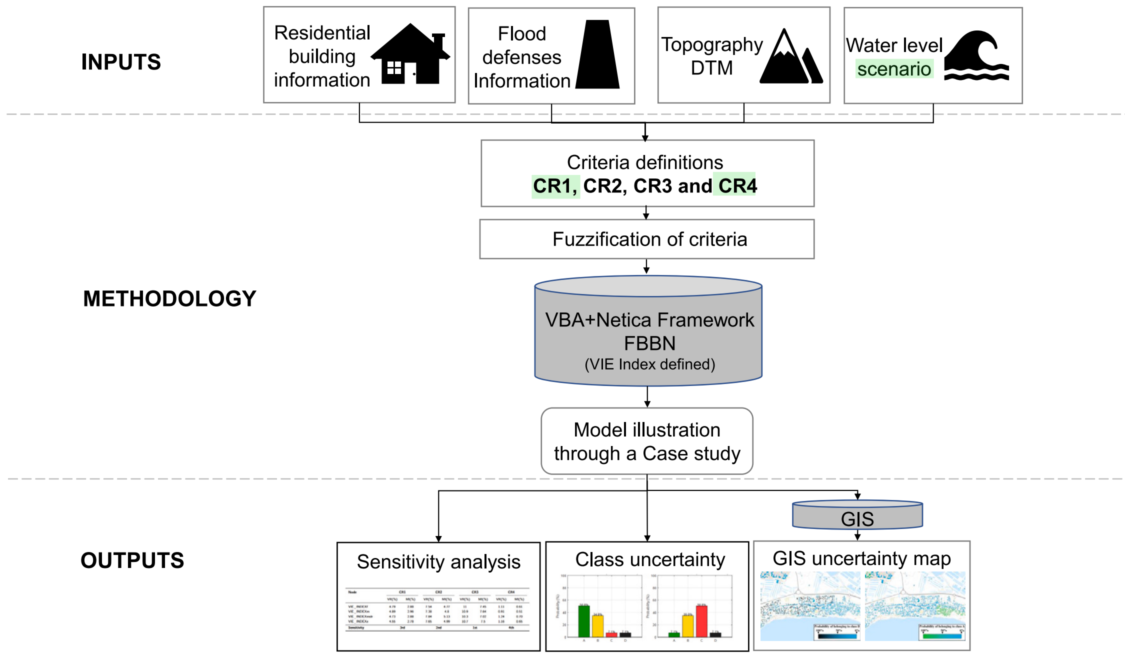

Fig. 2. Flowchart of the application of the methodology.

To overcome these limitations, this study proposes the integration of the VIE Index into a Fuzzy Bayesian belief network (FBBN). Separately, Bayesian Belief Networks (BBNs) have proven effective results in constructing robust probabilistic frameworks capable of representing interdependencies among variables and quantifying associated uncertainties. They have been widely applied in structural reliability, corrosion modeling, and flood risk assessment [18,19,38–41]. On the other hand, the fuzzy number addresses the vagueness and imprecision that are often present in the problem. By deriving fuzzy probabilities or likelihoods, it is possible to estimate the uncertainty even when the inputs are qualitative or partially known. This approach has been successfully applied in fields such as seismic risk assessment, oil & gas pipeline reliability [38,39,42,43] and flood risk assessment [44]. The proposed hybrid framework has the objective of using the inferential power of BBN, capable of modeling conditional dependencies and updating beliefs with new evidence, together with the flexibility of fuzzy logic, which enables the quantification of uncertainty from imprecise or categorical data. The result is a probabilistic model that offers a more realistic and adaptable representation of vulnerability in flood-prone residential environments.

2. Fuzzy Bayesian belief network methodology

2.1. Overview

Fig. 2 summarizes the proposed FBBN methodology. The inputs primarily consist of data related to the buildings of the area studied. This includes information on building typology, configuration, and vertical elevation that are essential for the calculations. Additionally, data on existing flood defense structures is also required, as the proximity of each building to these protective elements and the condition of the defenses [34] directly influence its vulnerability. A digital terrain model is also necessary to determine the ground elevation and understand the potential extent of floodwater, this includes accurate data on current sea levels in the coastal zone. Furthermore, information on flood scenarios is required. These scenarios are hypothetical but realistic representations of potential flood events, typically defined by return periods and grounded in historical and probabilistic analyses.

The proposed FBBN methodology uses the previously described input data to define four core criteria:

- CR1 (potential water depth),
- CR2 (proximity to flood defenses),
- CR3 (architectural typology), and
- CR4 (proximity to a rescue point).

While the detailed definitions and scoring of these criteria are explained in the following sections, it is important to note that the criteria highlighted in green (CR1 and CR4) are scenario-dependent. This means that their values vary across different flood scenarios, as they are directly influenced by water level conditions. In contrast, CR2 and CR3 are scenario-independent since they reflect static spatial and structural features. Once defined, all criteria are subjected to fuzzification using triangular membership functions to account for uncertainty in the input data. The fuzzified inputs are fed into a BBN model, where a VIE Index node is defined to reflect the resulting vulnerability based on combinations of the criteria. The model was implemented through a VBA+Netica computational framework, enabling the evaluation of various flood scenarios. Finally, the model was assessed through a case study to verify consistency with the original VIE framework and to illustrate the probabilistic outputs.

The outputs of the model include a sensitivity analysis to understand the behavior of the model, and both quantitative and spatial representations of flood vulnerability. First, a class uncertainty assessment is performed, illustrating the degree of uncertainty assigned to each residential structure to belong to a vulnerability category. This assessment highlights cases where classification is ambiguous due to uncertainty at the input parameters or overlapping category thresholds, and will be further detailed in later sections. Additionally, a GIS vulnerability map is generated offering a spatial visualization of the VIE Index values and associated uncertainty across the study area. This map provides a practical tool for urban planners, emergency managers, and decision-makers, enabling them to identify the most vulnerable zones and prioritize interventions while also considering the degree of confidence in the results.

2.2. Extreme intrinsic vulnerability: VIE index

This study accounts for flood vulnerability using the Extreme Intrinsic Vulnerability: VIE Index proposed by Creach et al. [35,45]. Designed to prevent future casualties caused by coastal flooding, particularly

Table 1
VIE Index methodology, criteria definition.
Source: Adapted from [45].

EXPOSURE TO COASTAL FLOOD EVENTS		
Criteria		Description
CR1	Potential Water-depth	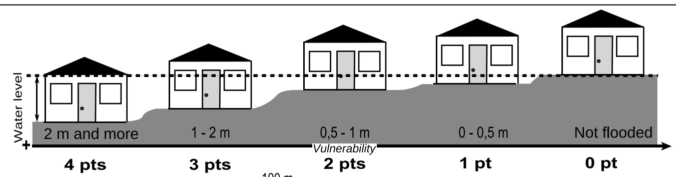
CR2	Distance to flood defenses	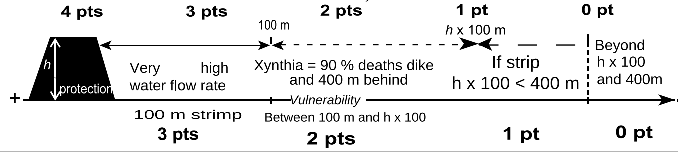
CHARACTERISTICS OF BUILDINGS		
Criteria		Description
CR3	Architectural type	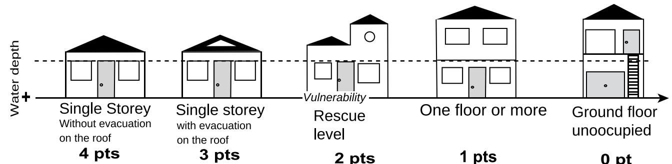
CR4	Closeness to rescue point	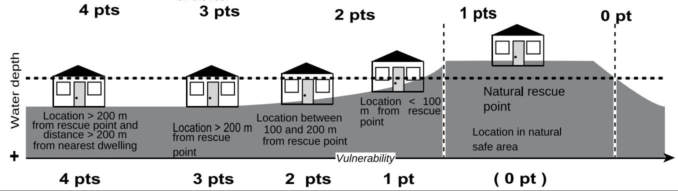

deaths by drowning, the VIE Index focuses on evaluating the vulnerability of residential buildings based on characteristics that influence the occupants ability to evacuate or remain safe during a flood event. This evaluation is based on four key criteria, detailed in Table 1, which reflect both the exposure of a house to flooding and the building's characteristics. CR1, CR3 and CR4 are scored from 0 to 4 and CR2 from 0 to 3, where 0 indicates minimal vulnerability and 4 denotes extreme vulnerability.

CR1 represents the potential water depth expected at the building during a flood. This value reflects both the intensity of the flood event and the elevation or topographic context of the building. Higher water depths result in greater vulnerability. This depth is calculated by making the difference between the ground and water levels based on the DTM from the French Litto-3D program (LiDAR survey), vertical accuracy of 20 cm [46]. CR2 measures the distance from the building to the nearest flood defense system. The effectiveness of this protection depends on: (i) the physical distance, (ii) the defense's height and condition and (iii) the presence of topographic depressions (a basin effect), which may accelerate localized flooding. These adjustments are considered by Creach et al. [35,45] by modifying CR2 with ± 0.5 points. CR3 characterizes the architectural type of the house describing how its physical configuration affects occupant safety. For instance, single-story houses without rooftop access are considered highly vulnerable, while multi-story buildings or those with designated rescue levels are assigned lower vulnerability scores due to the greater likelihood of successful vertical evacuation. Finally, CR4 quantifies the building's proximity to the nearest Natural Rescue Point (NRP), a high-elevation area or designated shelter that facilitates safe evacuation. As the distance to the NRP increases, particularly when the building is isolated or surrounded by flood-prone zones, the associated vulnerability score also increases.

The significance of the VIE index lies in its foundation on real-world conditions observed during the Xynthia event in France. It accurately captures the primary factors that contributed to individuals becoming trapped inside their homes during the flood. Once each criteria is evaluated, a numerical value is assigned to each one of them and the VIE index can be calculated as:

$$\mathrm{VIE} = \begin{cases} 0, & \text{if CR1} = 0 \\ \frac{2}{3}\mathrm{CR1} + \mathrm{CR2} + \mathrm{CR3} + \frac{1}{3}\mathrm{CR4}, & \text{elsewhere} \end{cases} \quad (1)$$

The weights for the four criteria in the VIE index were carefully chosen to avoid double-counting related data and to ensure a balanced assessment of vulnerability [35]. Since CR1 and CR4 both come from the same terrain data and are correlated, they are combined into a single topographic group with a 2/3 weight for CR1 and 1/3 for CR4. The other two criteria, CR2 (proximity to defenses) and CR3 (architectural typology), are independent and each given a full weight. This approach ensures the index fairly represents different aspects of vulnerability without overemphasizing elevation-based factors.

Based on the computed VIE index, each building is assigned to one of four vulnerability classes when all the information is available, as detailed in Table 2. These categories, represented by distinct color codes, serve not only to clearly communicate risk levels but also to support spatial visualization using GIS tools. For example, when a structure is not exposed to flooding (i.e., CR1 = 0), the associated risk to occupants is considered negligible, and the VIE Index is accordingly set to VIE = 0. This index enables the identification of high-risk areas on vulnerability maps, enhancing the practical value of the model for planners and decision-makers.

The boundaries for the four vulnerability classes (A, B, C, D) were determined by Creach et al. [35] through empirical adjustment to best predict death risk. Although initial class limits were explored using automatic clustering methods, these did not reliably separate the highest-risk buildings. Therefore, Creach et al. [35] manually refined the class boundaries based on the observed impacts of Storm Xynthia. This manual calibration improved the model's accuracy, capturing 25 of the 29 historical deaths within Class D.

This methodology has some challenges. The first involves the availability of data on architectural typology (CR3). If a building is safe

Table 2
Interpretation of vulnerability classes based on the VIE Index.

Class	Range	Meaning
Class A	VIE = 0	Buildings are not exposed to floods, and therefore, do not endanger people.
Class B	VIE = [1–5]	Buildings are of a suitable design to reduce risk to people during floods. The level of vulnerability for people is low.
Class C	VIE =]5–8]	The vulnerability of buildings to floods is high but nonlethal, except for children, older, or disabled people.
Class D	VIE =]8–12]	The vulnerability of buildings to floods is very high and could result in fatalities in the case of floods.
Class N	VIE = Null	Class not determined due to lack of information.

from flooding (CR1 = 0), CR3 becomes irrelevant. However, when CR1 > 0, CR3 is essential to assess risk. If CR3 is unknown, the VIE cannot be reliably calculated. To avoid misclassifications, when information is not available, such buildings are categorized as 'Non-Determined' (Category N) in the original methodology.

A second challenge concerns adjustments to CR2 (distance to flood defenses), which in the original methodology incorporate two correction factors: one for the structural condition of the defense and another for topographical context (the 'basin effect'). Although these refinements improve accuracy, they will be excluded from the proposed FBBN due to uncertainty and lack of consistent data on the structural condition of defense structures. As a result, our model uses only the base value CR2 without additional corrections.

A last challenge concerns the water depth estimation for CR1. The used methodology provides a conservative estimate of potential water depths, which aligns with the VIE index's focus on life safety by identifying the most critical possible water depths. However, it does not account for dynamic hydrodynamic processes, such as flow velocity or drainage effects, which could influence inundation patterns. Future research could incorporate advanced hydrodynamic models to improve the spatial accuracy of water depth estimates and better capture the complexity of coastal flooding.

2.3. Bayesian belief network-based flood vulnerability index

The proposed framework combines fuzzy logic and BBN. Fuzzy logic will be used to account for the uncertainty for each criteria of the VIE index. BBN will be implemented to propagate these fuzzy inputs in the evaluation of the VIE index and to estimate the probability of belonging to each vulnerability class presented in Table 2. This section begins by presenting the coastal flood scenarios that are related to the criteria CR1 and CR4. Afterwards, the fuzzy and BBN components of the proposed approach are presented.

2.3.1. Flood hazard intensity

In order to account for the variability in flood hazard intensity due to different return periods and potential climate change impacts, this study considers four flooding scenarios. These scenarios are defined according to the recommendations a French ministry [47] for implementing the European Flood Directive [48]. The selected scenarios and their associated return periods are shown in Table 3. The Frequent, Medium, and Extreme scenarios use water levels estimated by regional authorities for Fromentine, which is near the study area [49]. Additionally, Table 3 includes a scenario based on the Medium water level, increased by a 60 cm sea-level rise projected for 2100. This +0.6 m value is a conservative regulatory standard recommended by the French observatory on climate change effects [47], ensuring that risk prevention plans align with long-term trends identified in IPCC reports.

2.3.2. Fuzzification of VIE index criteria

Fuzzy logic is a mathematical framework based on fuzzy set theory, first introduced by Lotfi Zadeh in 1965 [50]. Unlike classical binary logic that assigns elements a strict true or false value (1 or 0), fuzzy logic allows for partial membership in a set. This provides a systematic way to translate qualitative terms (e.g., 'low', 'medium', 'high') into numerical representations, allowing uncertainty, vagueness, and imprecision, often present in real-world systems, to be incorporated into modeling. Fuzzy logic is particularly useful when system boundaries are not well-defined, data is imprecise, or expert judgment must be included, as is often the case in risk assessment applications [51].

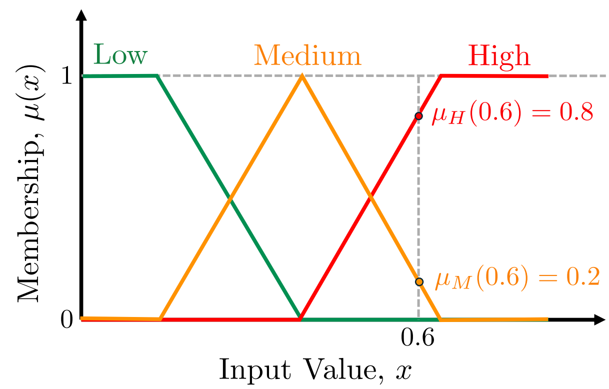

Fig. 3. Fuzzy membership example, Triangular function.

Each fuzzy set is defined by a membership function, which determines the degree of membership of a given input to a qualitative category. These functions can take various shapes such as triangular, trapezoidal, or Gaussian, depending on the system requirements and available data [52]. In this research, triangular membership functions are predominantly used due to their simplicity and computational efficiency. The mathematical formulation of a triangular membership function is defined as:

$$\mu(x) = \begin{cases} 0, & x \le a \text{ or } x \ge c, \\ \frac{x-a}{b-a}, & a < x \le b, \\ \frac{c-x}{c-b}, & b < x < c. \end{cases} \tag{2}$$

This function computes the degree of membership μ of an input value x within a fuzzy category, defined by the parameters a, b, and c, which respectively represent the lower bound, the peak and the upper bound of the triangle. To illustrate the concept, Fig. 3 shows a basic example of a fuzzy membership function composed of three categories: Low (L), Medium (M), and High (H). The low membership function has a linear falling slope function represented by:

$$\mu_L(x) = \begin{cases} 1, & x \le b, \\ \frac{c-x}{c-b}, & b < x < c, \\ 0, & x > c. \end{cases} \tag{3}$$

The high membership function has a linear rising slope as:

$$\mu_H(x) = \begin{cases} 0, & x \le a, \\ \frac{x-a}{b-a}, & a < x \le b, \\ 1, & x > b. \end{cases} \tag{4}$$

Suppose that a value of 0.6 is evaluated for a parameter studied. According to the defined triangular membership functions, the degrees

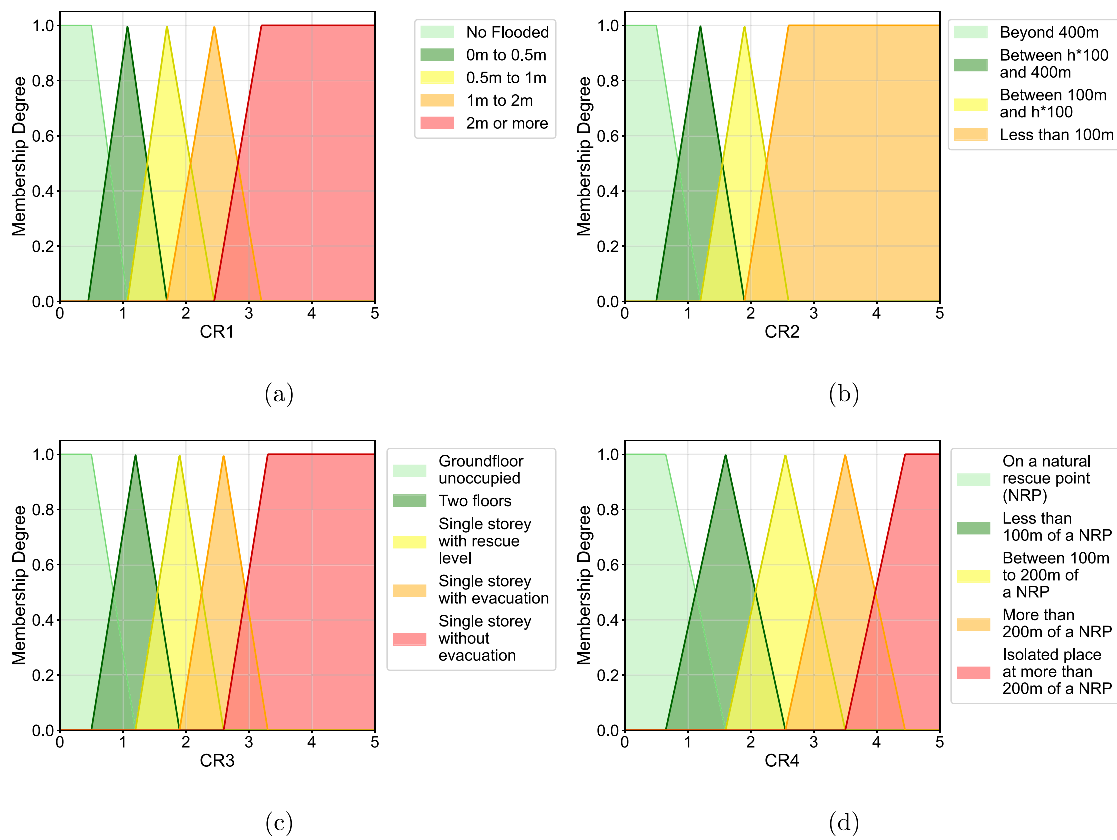

Fig. 4. Fuzzy memberships for (a) CR1: Potential water depth, (b) CR2: Distance to flood defenses, (c) CR3: Architectural type and (d) CR4:Closeness to rescue point.

of membership would be $\mu_L(0.6) = 0$, $\mu_M(0.6) = 0.8$, and $\mu_H(0.6) = 0.2$, summarized as $(\mu_L, \mu_M, \mu_H) = (0, 0.8, 0.2)$, indicating that the input partially belongs to both Medium and High categories simultaneously (Fig. 3).

The original VIE formulation assigns qualitative parameters with their corresponding crisp categorical values to each criterion (Table 1). While these thresholds defined by the original methodology are grounded in data from the real Xynthia event, they inherently carry a degree of uncertainty that is not captured in a deterministic model. For example, although buildings classified with CR3 = 4 (single-story homes with no rooftop evacuation possibility) are considered extremely vulnerable, historical data from Storm Xynthia reveals that such conditions did not uniformly lead to fatalities. Approximately 75% of the victims were indeed trapped in these building types [7,11], but the remaining 25% were distributed across other architectural categories, indicating overlapping vulnerabilities and uncertainty in the classification. Similarly, CR2 (distance to flood defenses) also demonstrates variability. Around 90% of fatalities occurred within 400 m of a dike [11], which includes classifications CR2 = 1, 2, or 3. However, the precise risk associated with each of these categories is not sharply defined; rather, there is a continuous gradation in vulnerability that cannot be fully represented using crisp boundaries alone.

This study introduces a fuzzification process for the four vulnerability criteria: CR1 (potential water depth), CR2 (distance to flood defenses), CR3 (architectural typology), and CR4 (closeness to a rescue point), as shown in Fig. 4. The values of the parameters of these membership functions of this figure are detailed in Appendix (Table A.7). These membership functions preserve the original categorical structure defined in the VIE methodology but introduce smooth transitions between states. This choice is justified because fuzzy logic:

- enables the representation of uncertainty in the input criteria. The inputs used to compute the VIE Index (Table 2) are difficult to define with clear thresholds and are subject to epistemic uncertainty.
- improves the realism of modeling by avoiding abrupt transitions between vulnerability classes, instead enabling gradual and continuous changes that more accurately reflect the complexity of residential flood vulnerability.
- integrates naturally with BBN by fuzzifying the inputs before feeding them into the BBN structure.Consequently, the proposed model will preserve uncertainty and variability supporting more robust and interpretable inference.

Membership values were assigned such that the maximum membership value (1) corresponds to the discrete points of the input parameters, with smooth transitions between adjacent classes. The boundaries were set to ensure that membership values overlap appropriately, maintaining a sum of 1 between two neighboring classes.

2.3.3. Bayesian belief network

A BBN is a probabilistic graphical model that represents a set of random variables and their conditional dependencies through a visual diagram called a Directed Acyclic Graph (DAG) [53]. In this structure, the main components are nodes and edges; each node corresponds to a variable, and each edge represents a direct probabilistic dependency between the connected nodes. Bayesian Belief Networks are built upon Bayes theorem, which allows the computation of the posterior probability $P(X_1 \mid X_2)$ based on prior knowledge:

$$P(X_1 \mid X_2) = \frac{P(X_2 \mid X_1) \cdot P(X_1)}{P(X_2)} \quad (5)$$

Table 3
Considered coastal flood scenarios.
Source: Adapted from [35,36].

Scenario	Acronym	Return Period	Sea Water Level at Fromentine Town
Frequent	fr	10 years	3.6 m NGF[b]
Medium	m	100-300 years	4.2 m NGF
Medium + SLR[a]	mslr	Same as above +0.6 m	4.8 m NGF
Extreme	ex	1000 years or more	5.2 NGF

[a] SLR: Sea level rise.
[b] NGF: French general level.

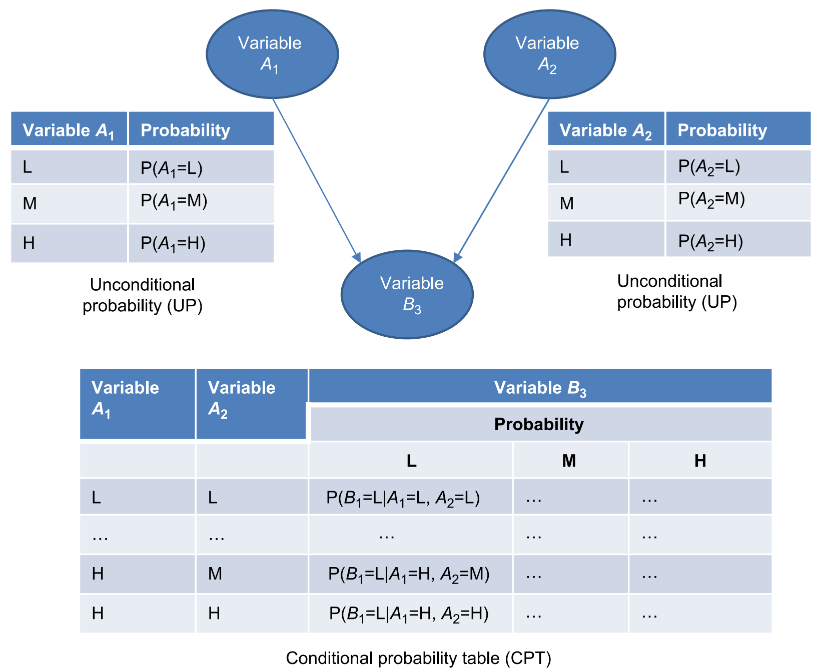

Fig. 5. Example of a basic BBN.
Source: Adapted from [43]

Eq. (5) expresses the probability that an event (X_1) occurs given that another related event (X_2) has already occurred. It enables the network to update its beliefs when new information becomes available. Bayesian Networks encode the joint probability distribution of a set of N variables as the product of their conditional probabilities, according to the chain rule of BBNs:

$$P(\mathbf{X}) = P(X_1, \dots, X_N) = \prod_{i=1}^{N} P(X_i \mid \mathrm{pa}_i) \tag{6}$$

where pa_i denotes the set of parent nodes of X_i. A parent node is a variable that directly influences another, and is represented by an outgoing edge in the DAG. Conversely, a child node is influenced by one or more parents and is identified by one or more incoming edges. For example, in Fig. 5, A_1 and A_2 are the parent nodes of B_3. Understanding the relationship between parent and child nodes is fundamental in BBNs. Nodes without parents like A_1 in Fig. 5, are defined by a marginal probability distribution, while child nodes such as B_3, are characterized by joint probability distributions influenced by their parents. Each node is associated with a probability table. This table takes the form of a Conditional Probability Table (CPT) for child nodes and an Unconditional Probability Table (UPT) for root nodes with no parents.

The behavior and output of a BBN is sensitive to the values assigned in these probability tables, making their accurate definition critical to the model's performance [54]. Several methods exist to populate these tables. They can be derived through expert elicitation [55], based on training data [56], or, as in this study, computed directly from a governing equation that defines the structure and interactions of the model [57]. This equation-based approach ensures consistency and transparency in the relationship between input criteria and the outcomes.

The structure of the developed FBBN used to assess the flood vulnerability index is illustrated in Fig. 6. The input values assigned are based on the fuzzy memberships for each corresponding criterion defined in Fig. 4. This FBBN includes the four flooding scenarios outlined in Table 3. For each scenario, the parent nodes (CR1, CR2, CR3, and CR4) represent the key vulnerability criteria contributing to the computation of the VIE Index. These nodes are defined using categorical states, consistent with the classifications presented in Table 1.

The VIE index is the child node and aggregates the influence of its respective parent nodes through CPTs populated applying Eq. (1). As a result, four parallel branches are constructed, one for each flooding scenario. It is important to note that the nodes CR2 and CR3 are shared across all scenarios, as the distance to flood defenses and architectural typology are constant for a given building and do not vary with the scenario. In contrast, CR1 (potential water depth) and CR4 (closeness to a rescue point) are scenario-dependent variables, as both are influenced by the severity of flooding and thus vary according to water depth in each considered case.

2.3.4. Sensitivity analysis of the Bayesian belief network model

BBN model outputs of the VIE Index are influenced by the input parameters (parent node) and *a priori* assigned conditional probabilities. Thus, there is a need to carryout sensitivity analysis to identify

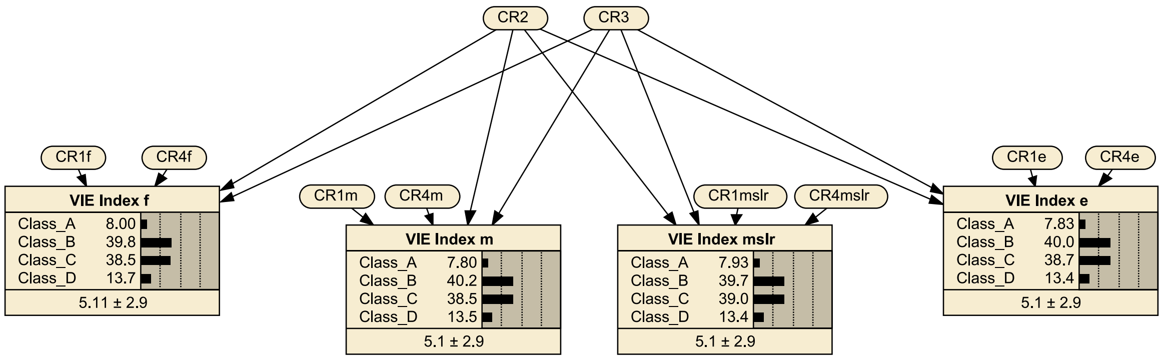

Fig. 6. Architecture of the proposed FBBN framework.

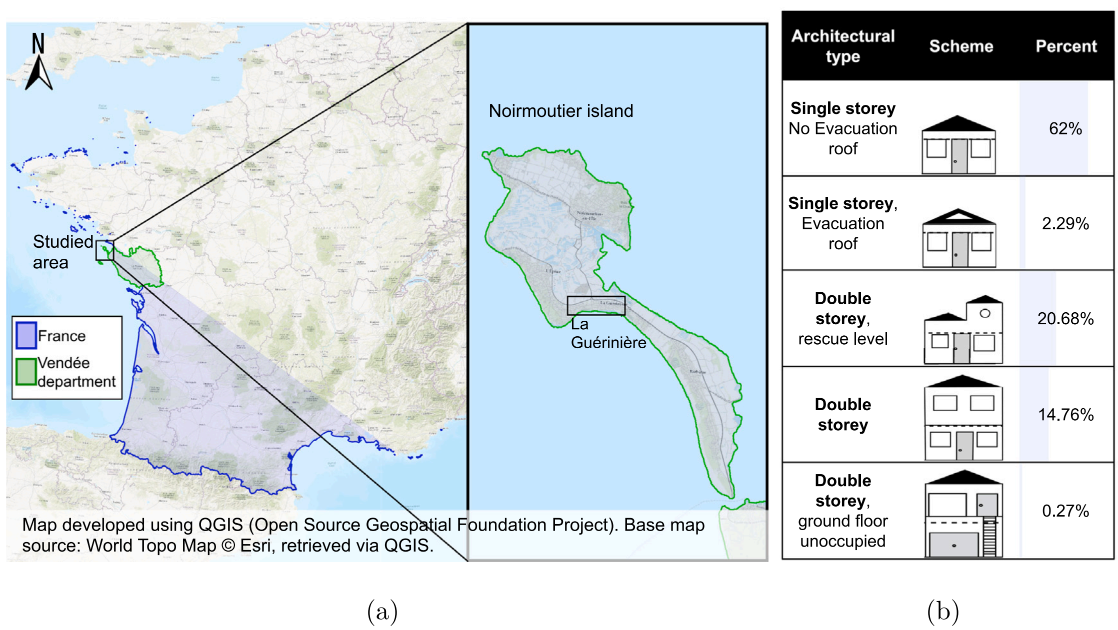

Fig. 7. Characterization of the case study. (a) Location of the Noirmoutier island, Vendée department, (b) Architectural type distribution in Noirmoutier island.

critical input parameters that have significant impact on the VIE Index. Results of the sensitivity analysis, for example, can aid decision makers in prioritizing and collecting reliable data for the influential (sensitive) parameters and leave the least sensitive as unknown *a priori* state. In this paper, variance reduction method [58] is used to quantify the sensitivity of the VIE Index to its parent nodes (CR1 to CR4). This method measures the change in the variance of the expected value of a target node when new evidence is introduced in one of the input variables, and is computed as [59]:

$$V(q|f) = \sum_{q} p(q|f)\left(X_q - E(Q|f)\right)^2 \tag{7}$$

where q denotes the states of the target node Q, $p(q|f)$ is the conditional probability of q given evidence f on node F, X_q is the numeric value associated with each state, and $E(Q|f)$ is the expected value of the target after the finding.

With the BBN network shown in Fig. 6, for example, the parent nodes that contribute directly to *frequent* scenario are CR1f, CR4f, CR2, and CR3; whereas, for *medium* scenario, the nodes are CR1m, CR4m, CR2, and CR3. CR2 and CR3 are shared across all scenarios, whereas, CR1 and CR4 have scenario-specific versions (e.g., CR1e, CR1m, CR1f, CR1mslr), and their influence is analyzed within the context of their respective flood condition.

The results of the variance reduction are computed, first, by varying the states of each VIE Index. For example, for VIE Index f, in the *priori* state, the variance is 2.9, and varying each node, state of the nodes are updated, the cumulative variance is 8.502. This will be the basis used in the percent of variance reduction calculation for VIE Index f. Subsequently, keeping all nodes in their unknown states, the variance reductions are computed by varying the state of each node of interest. Table 4 summarizes percentage of variance reduction for the four vulnerability criteria (CR1 to CR4). Results across the four flood scenarios consistently show that CR3 (architectural typology) has the highest contribution within 10 to 11% variance reduction in all scenarios, followed by CR2 (distance to defenses) around 7% and CR1 (potential water depth) with about 4%. On the contrary, CR4 (closeness to rescue point) had limited influence in all cases, below 1.5% in all cases. These findings validate the internal structure of the fuzzy BBN model, confirming that the VIE Index is most sensitive to the physical vulnerability of the building and its exposure to flooding. This justifies prioritizing architectural retrofitting and flood protection measures in subsequent adaptation strategy simulations.

3. Results and discussions

3.1. Case study: Noirmoutier island

This work studies the vulnerability of the island of Noirmoutier that is located on the Atlantic coast of France. Administratively part of the Vendée department (Fig. 7(a)), Noirmoutier covers an area of

Table 4
Variance reduction for each scenario.

Node	Scenario	CR1 (%)	CR2 (%)	CR3 (%)	CR4 (%)
VIE Index f	Frequent	4.79	7.54	11.0	1.11
VIE Index m	Medium	4.89	7.38	10.9	0.91
VIE Index mslr	Med. + sea Level rise	4.73	7.84	10.3	1.24
VIE Index e	Extreme	4.55	7.65	10.7	1.16
Sensitivity Rank		**3rd**	**2nd**	**1st**	**4th**

Table 5
Number of houses per class for the four studied scenarios.

Class	Frequent		Medium		Med.+sea level rise		Extreme	
	Count	%	Count	%	Count	%	Count	%
A	12641	60.06%	10021	47.61%	7921	37.64%	6587	31.30%
B	2099	9.97%	2630	12.50%	2600	12.35%	2220	10.55%
C	3254	15.46%	4135	19.65%	5052	24.00%	5281	25.09%
D	375	1.78%	767	3.64%	865	4.11%	1029	4.89%
N	2677	13%	3493	17%	4608	22%	5929	28%
TOTAL	21046	100%	21046	100%	21046	100%	21046	100%

approximately 48 km^2 and is composed of ten localities grouped into four municipalities. Noirmoutier Island was selected due to its insular nature, low elevation and significant number of one-storey houses which makes it particularly vulnerable to coastal flooding. Noirmoutier Island has suffered the impact of coastal erosion for more than a century, forcing its inhabitants to raise protection structures from the sea since 1770. For this reason, the island nowadays is protected by 24 km of flood defenses (i.e., sand barriers, dunes, riprap, groynes and other measures) on its east and west coasts [60].

The data used in this study were obtained from the database developed and made available in [61]. This database contains information on more than 21,000 residential buildings across the island (Table 5). It includes details on defense structures, water level elevations, natural rescue points, and house typology, all of which are necessary to determine the VIE index. Architectural type information is incomplete for 59.5% of the houses on the island. Although this percentage is high, it is important to note that many of these houses are already classified as Class A (CR1 = 0), meaning they are outside the flood envelope and not exposed to potential flooding. Table 5 also shows the number of houses included in the analysis for each scenario, as well as those assigned to 'Category N' due to missing data. Depending on the scenario, Category *N* buildings represent between 13% and 28% of the total housing stock.

The architectural type of the houses in the island is distributed as shown in Fig. 7(b). Most houses (64.29%) have one floor. This architectural type leads to a higher vulnerability against a flood event. Only 35.71% of houses have two levels. Additional characteristics of the island include the population and residential urbanization that since 1968 have increased by 19%, and +162%, respectively [45]. This important growth is mainly due to the construction of leisure residential houses, that corresponded to a 50% in 2011 [62].

Table 5 summarizes the distribution of houses across different vulnerability classes for each scenario. These results were determined using the raw database and Eq. (1). In the frequent scenario, approximately 70% of houses fall within the safer categories (A and B). However, this proportion declines to about 42% under the extreme scenario, illustrating the significant impact of elevated seawater levels and extreme events. Correspondingly, the number of houses classified in the more dangerous categories (C and D) increases in the extreme scenario, highlighting the heightened risk to the built environment under severe climate conditions.

3.2. Comparison with the previous methodology

The original methodology developed by Creach et al. [35,45] computes a unique value for each residential building to classify the house in a vulnerability class from A to D. The results of this classification are provided in Table 5. In contrast, the proposed FBBN framework gives as output the probability distribution of each building's likelihood of belonging to each class from A to D, quantifying the uncertainty associated with the classification. This probabilistic output is the core strength of the proposed FBBN framework because it allows us to explicitly quantify how a building fits into one category while acknowledging its potential association with others.

This section compares the results of both the original and FBBN methodologies. This comparison assesses how aligned both approaches are and whether the results fall within similar vulnerability ranges. However, since we are comparing deterministic and probabilistic outputs, the results obtained using the FBBN method are transformed with a weighted sum, using a sum product operation between the four probabilities obtained. Therefore, a single 'global value' is calculated per building. This value estimates the vulnerability of each building and facilitates its comparison with the original results.

Fig. 8 compares the global values obtained using the FBBN with those estimated using the original deterministic model developed by Creach et al. [35,45] for all four scenarios. The strong alignment between the results obtained for the two models confirms the consistency and robustness of the proposed FBBN probabilistic framework. Similar patterns were observed for all flooding scenarios, each showing a high degree of alignment with their corresponding results from the original methodology.

An important question arises regarding the class boundaries. In the original model, crisp thresholds were defined for each vulnerability class (A to D); however, these thresholds could differ when propagating uncertainty using the proposed FBBN model. FBBN class boundaries were therefore calculated to ensure consistency with the original VIE classification. The recalculation method involves determining new boundary values that maximize the number of buildings remaining in the same class as identified by the original VIE classification. This approach ensures that the majority of buildings classified under a specific class in the original VIE framework are similarly classified under the FBBN framework, maintaining alignment between the two methods. Consequently, Fig. 8 also includes the class boundaries for the purpose of visual comparison and consistency check of class alignment. Red vertical dashed lines represent the boundaries proposed by the original methodology (also described in Table 2), and blue horizontal dashed lines represent the computed class boundaries of the FBBN in 0, 2, 4.5, 7.5 and 12. The colored zones (A to D) highlight areas where both methods assign the same vulnerability class, indicating alignment. It is observed that few points fall outside these zones suggesting that, for these buildings, the classification has some

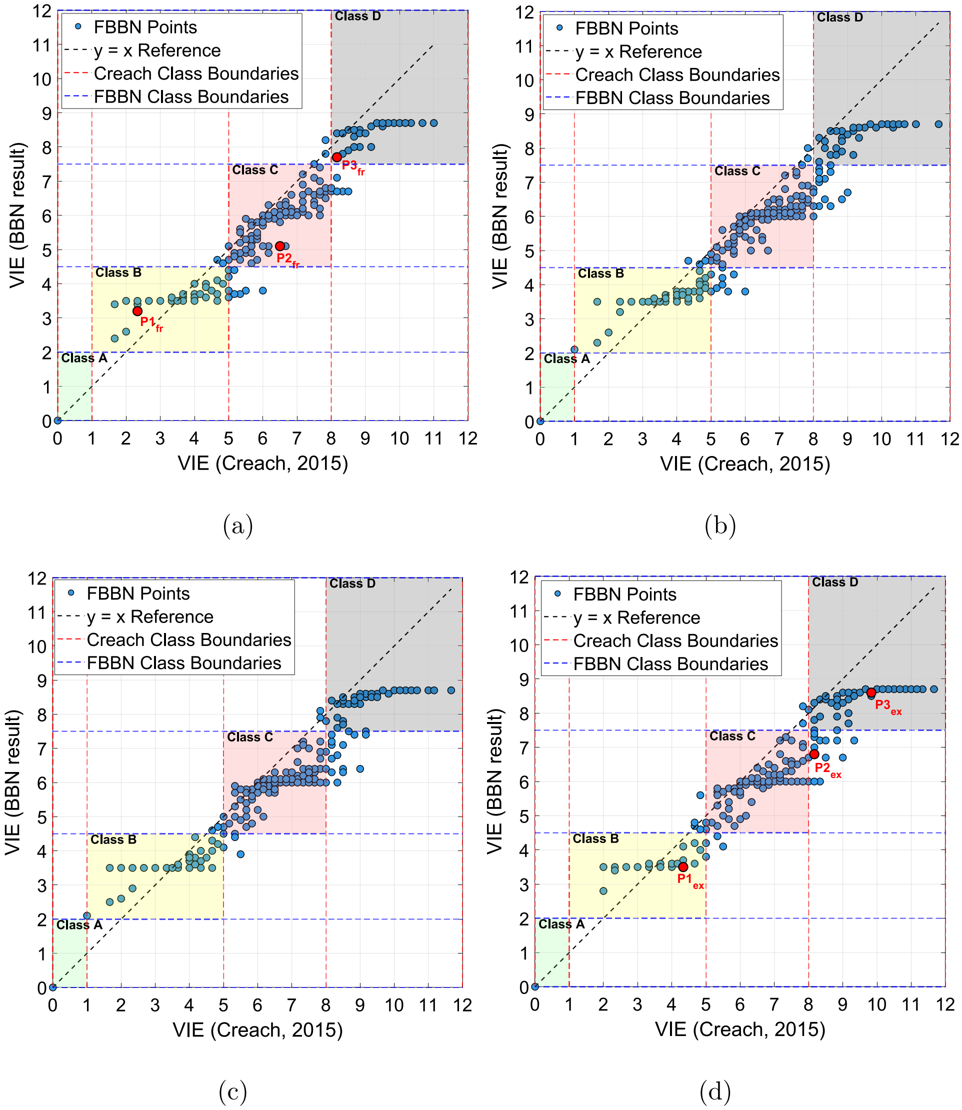

Fig. 8. Comparison of results obtained from the FBBN framework with those of the original methodology for the scenarios described in Table 3. Detailed results for the sample points P1, P2 and P3 are provided in Fig. 10. (a) Frequent scenario,(b) Medium scenario, (c) Medium + SLR scenario,(d) Extreme scenario.

Table 6
Number and percentage (between brackets) of outliers per scenario when comparing FBBN and Creach et al results.

Class	Frequent	Medium	Medium + SLR	Extreme
Outliers	305 (1.45%)	427 (2.03%)	552 (2.62%)	514 (2.44%)

outliers. Table 6 presents the number of outliers per scenario. The number of buildings falling outside these zones remains below 3% (with respect to the total number of buildings) for the four scenarios. This small percentage confirms the ability of the FBBN framework to classify the vulnerability of these buildings when considering various flooding scenarios. This visualization is intended not as a strict quantitative validation, but rather as a consistency check to ensure that the FBBN model preserves the general structure of the original classification. While this consistency check confirms that the FBBN replicates the original VIE framework probabilistically, it does not constitute a full validation of the model. Unfortunately, due to the lack of access to independent empirical data, such as damage records, insurance claims, or mortality data, a full validation could not be performed in this study. Future work should focus on validating the FBBN framework against independent datasets to further assess its reliability and applicability in real-world scenarios.

3.3. *Sensitivity analysis of membership function values*

To evaluate the impact of the selected membership function values on the FBBN framework, a sensitivity analysis was conducted. The purpose of this analysis was to assess the robustness of the fuzzification process and its influence on the VIE BBN classification results. Specifically, we compared the baseline membership values provided in Fig. 4 with alternative membership values that introduced adjusted boundaries. The membership functions for both cases were designed to ensure smooth transitions between classes, with overlaps guaranteeing that the sum of membership values equals 1 between adjacent classes. For this sensitivity analysis the frequent scenario was selected for 22,000 buildings and the values for the membership functions for both cases are detailed in Table A.7.

The results of the VIE BBN values for both cases are compared in Fig. 9. The horizontal axis represents the VIE values estimated by Creach

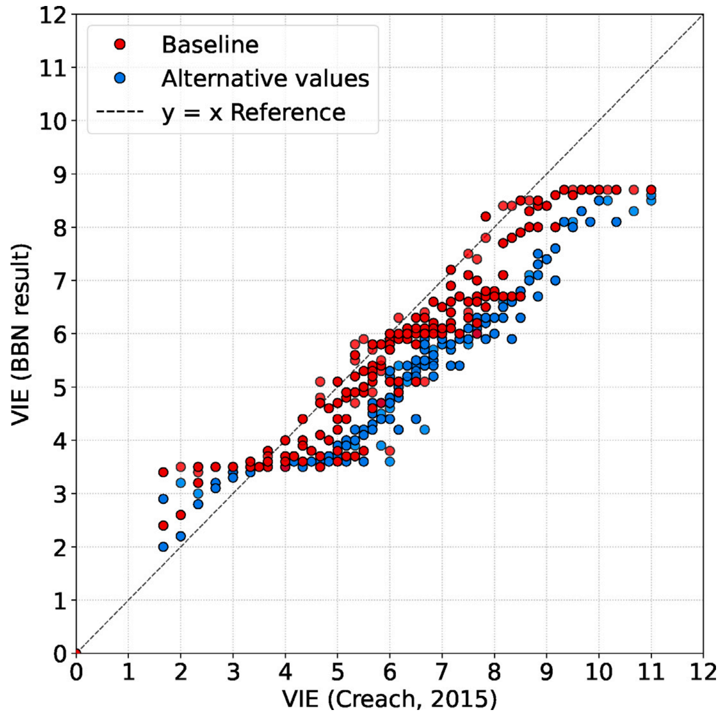

Fig. 9. Comparison of results obtained from the FBBN framework with those of the original methodology considering two sets of membership function values: baseline and alternative values.

(2015), while the vertical axis shows the VIE BBN values computed in this study. The comparison indicates that the baseline membership values (red points) provide better alignment with the analytical VIE values compared to the alternative membership values (blue points). However, both cases slightly underestimate the analytical VIE values. If the objective is to achieve an exact match with the original VIE results, further optimization of the membership functions, such as through likelihood maximization, would be necessary. Nevertheless, the results demonstrate that the VIE BBN classification remains stable and consistent across the tested cases, confirming the reliability of the fuzzification approach. Future work will focus on optimizing the membership functions using advanced methods, such as Adaptive Neuro-Fuzzy Inference Systems, and validating the framework against independent datasets to further enhance its accuracy and applicability.

3.4. Probability of belonging to each vulnerability class

The proposed FBBN allows us to determine the probability of belonging to each vulnerability class. This probability is illustrated for three sample points (P1, P2, and P3) that were selected from the scatter-plots presented in Fig. 8 for the frequent (Fig. 8(a)) and extreme (Fig. 8(b)) scenarios. The points (P1, P2, and P3) correspond to the same buildings but under different flooding scenarios. It is observed that all three points shift toward the upper right side of the graph. This behavior is expected, as the flooding scenarios progress from frequent to extreme (see Table 3), resulting in more severe conditions. The increased severity raises the water level, which in turn places the building in a more vulnerable state. Setting aside these 'global values' calculated for each point, the corresponding output probability distributions are presented in Fig. 10. These graphs illustrate how the FBBN model allocates likelihoods across different vulnerability classes based on the input values.

For P1, which has a low VIE score, under a frequent scenario (Fig. 10(a)), the probability is concentrated in classes A and B, indicating low vulnerability. However, when the same building is subjected to an extreme flooding scenario (Fig. 10(d)), the distribution shifts noticeably, and the building has a very high probability of belonging to class B.

P2 exhibits a mid-range VIE score. Under a frequent scenario (Fig. 10(b)), the highest probability is associated with class C. However, it is noteworthy that there is also a significant probability that the building belongs to class B. In contrast, for the same building under an extreme flooding scenario (Fig. 10(e)), the probability of belonging to class C increases, and there is also a considerable likelihood that the building falls into the most vulnerable category, class D. These results are meaningful for quantifying uncertainty: while the original methodology would have produced a single, crisp classification of the house in category D, our approach reveals uncertainty that shifts the probabilities toward class C.

For P3, which has a high VIE score, the probability distribution under a frequent scenario (Fig. 10(c)) is concentrated mostly in Classes C and D, reflecting a high level of vulnerability. As anticipated, when considering an extreme flooding scenario (Fig. 10(f)), the probability shifts further toward class D, indicating that the building is increasingly likely to fall into the most vulnerable category under more severe conditions. These probabilistic representations provide a richer and more informative basis for decision-making than single deterministic classifications.

3.5. Geo-spatial representation of vulnerability and uncertainty

In this section, we examine the spatial distribution of vulnerability within the study area. We begin by comparing the classification results obtained from the original VIE index with those produced by the proposed FBBN approach. This comparison allows for a direct visual assessment of both the similarities and differences between the two methodologies throughout the study area. Fig. 11 provides a spatial comparison of vulnerability classifications for the same residential zone (La Guérinière town) highlighted in Fig. 7 on the Noirmoutier Island. The results correspond to the frequent flood scenario and represent the 'global value' for the FBBN approach. Fig. 11(a) shows the results from the original deterministic methodology, while Fig. 11(b) presents the classifications generated by the FBBN model. It is important to note that, although Fig. 11 focuses on a small section of the island in La

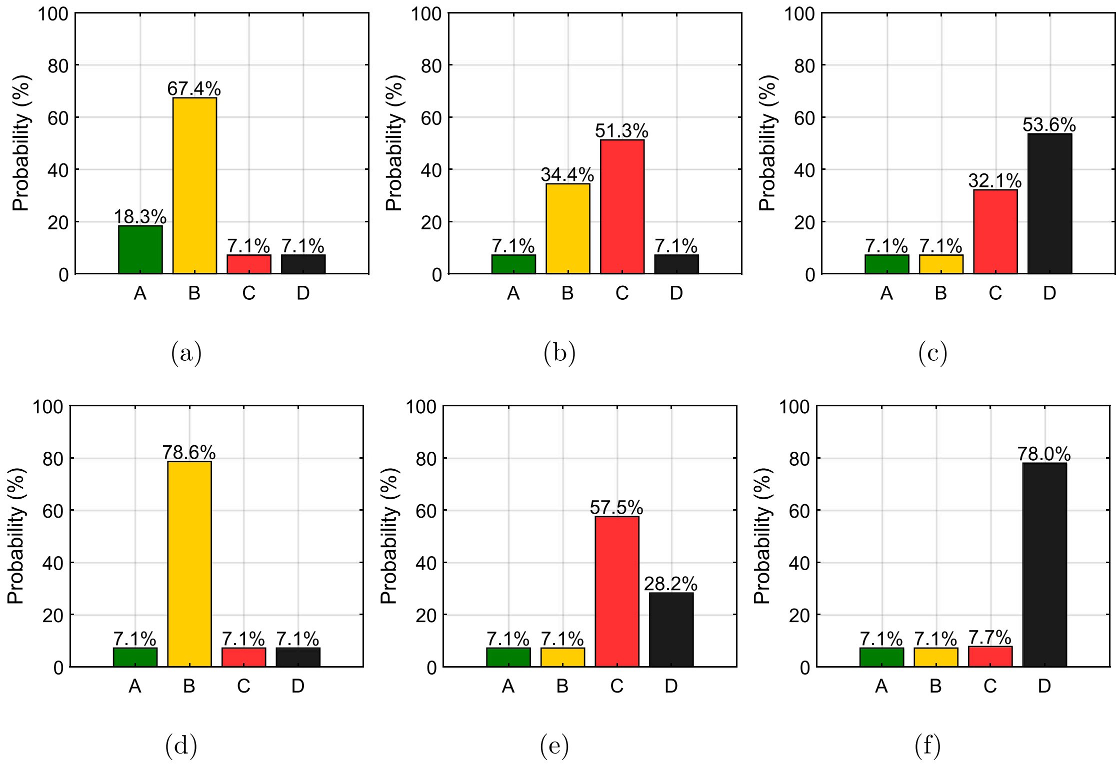

Fig. 10. Probability of belonging to each class for the three sample points presented in Fig. 8 and frequent and extreme scenarios. (a) Point P1, frequent scenario, (b) Point P2, frequent scenario, (c) Point P3, frequent scenario (d) Point P1, extreme scenario, (e) Point P2, extreme scenario,(f) Point P3, extreme scenario.

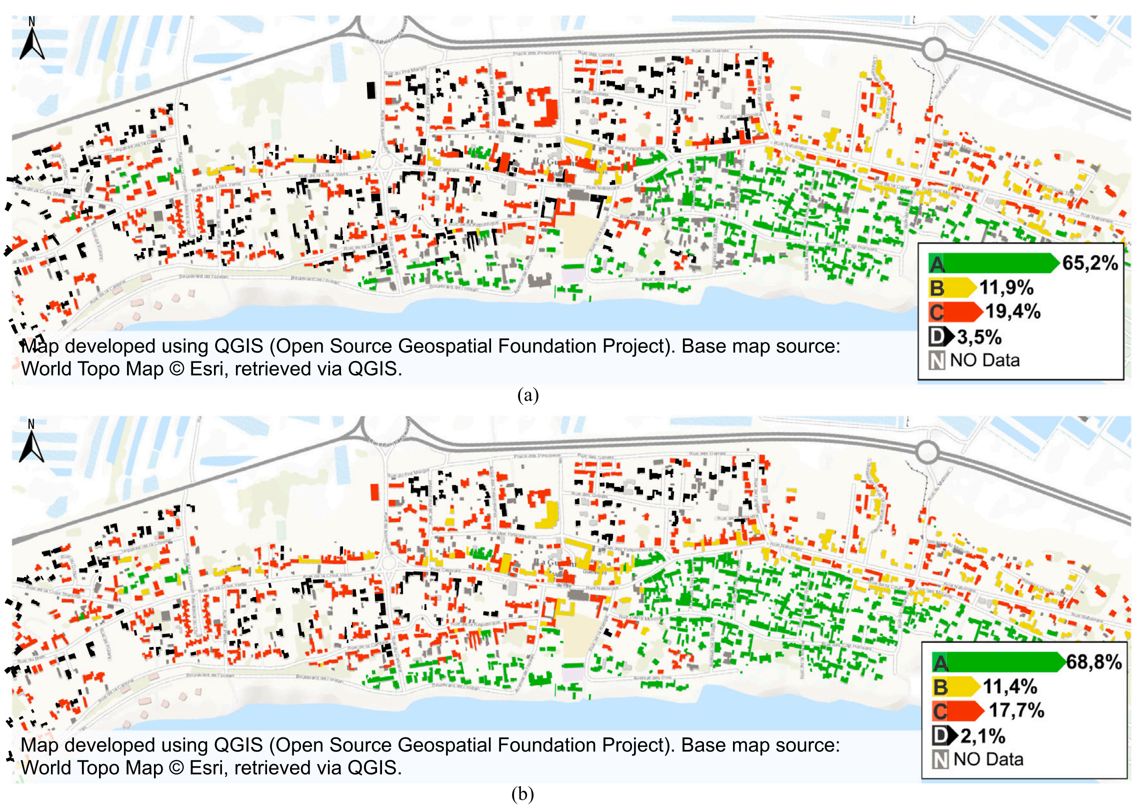

Fig. 11. Comparison of vulnerability results for La Guérinière town considering the frequent flood scenario: (a) Original VIE index [61], (b) FBBN approach.

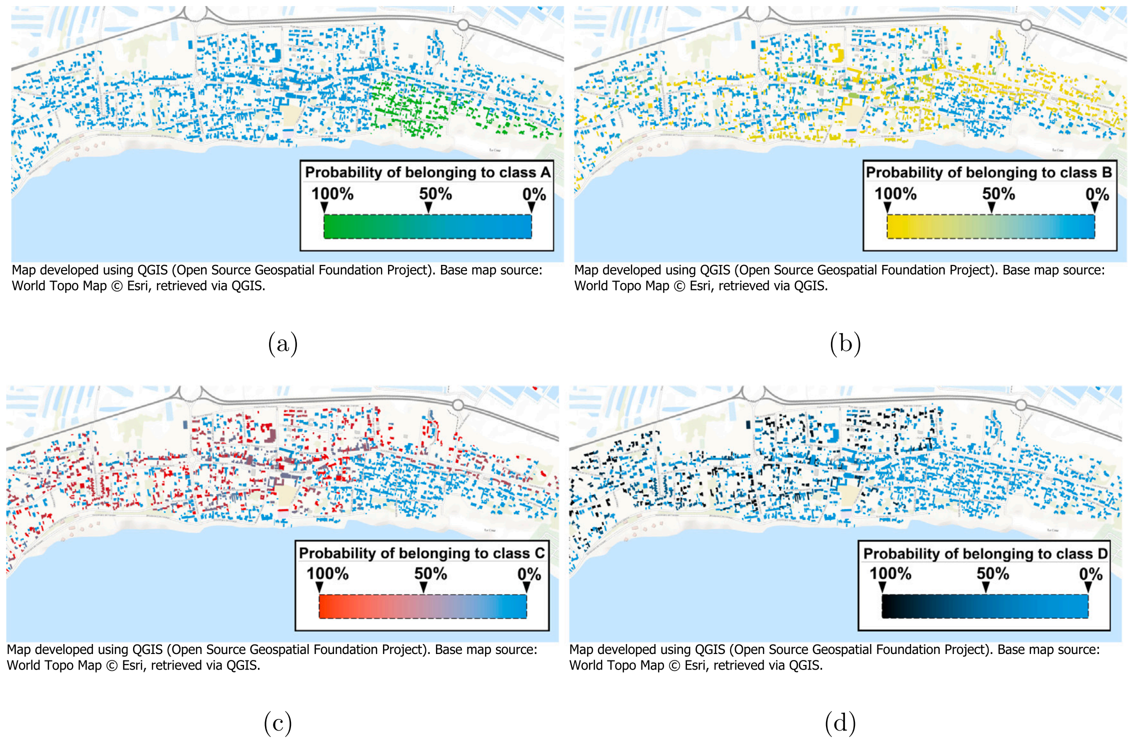

Fig. 12. Output probability result for frequent scenario, Each map shows the probability of a building belonging to a given vulnerability class, ranging from 0% (low certainty) to 100% (high certainty). (a) Probability of being in A, (b) Probability of being in B, (c) Probability of being in c and (d) Probability of being in D.

Guérinière town, the percentages shown in the labels correspond to the entire island.

According to the values presented in Fig. 11, the FBBN approach introduces a slight shift in the distribution of vulnerability classes. Notably, the proportion of buildings classified as Class D (highest vulnerability) decreases from 3.5% in the original model to 2.1% in the FBBN results, while the percentage of buildings classified as Class A increases from 65.2% to 68.8%. This suggests that the FBBN model marginally reduces the concentration of buildings in the highest-risk category. This behavior is likely attributable to the model's ability to capture epistemic uncertainty and better reflect ambiguous or borderline cases. Unlike the original model, which applies rigid, deterministic thresholds to classify buildings, the FBBN enables probabilistic blending across class boundaries, helping to soften transitions between classes and reduce the likelihood of misclassification for structures with input values near threshold limits. The proportion of buildings in Class B remains virtually unchanged, while Class C exhibits a slight decrease. Overall, the spatial distribution patterns remain largely consistent between both models, reaffirming the internal coherence of the FBBN but demonstrating its added value in explicitly representing uncertainty.

Furthermore, a second visualization has been developed to illustrate the uncertainty in the classification of individual buildings. Fig. 12 presents the probabilities of belonging to each vulnerability class (A to D). In these maps, the probability to belonging to each class increases once the color is close to its characteristic color as defined in Table 2. The blue color quantifies the uncertainty regarding this classification. Visually, the maps illustrate that high confidence classifications, such as deep green for Class A or deep black for Class D, tend to cluster in spatially coherent areas reflecting the underlying spatial autocorrelation often present in a given geographic data. In contrast, lighter shades indicate locations where the model is less certain about class membership, effectively communicating the degree of uncertainty through color intensity. The results of this approach allows stakeholders to prioritize interventions not only based on predicted vulnerability but also on the reliability of the classification, supporting more informed and targeted decision-making.

4. Conclusions and perspectives

This study introduced a FBBN approach to enhance the VIE Index methodology for vulnerability assessment at the residential level. By integrating fuzzy logic and Bayesian belief networks, we addressed key limitations of the original deterministic framework, particularly its inability to represent uncertainty and conditional dependencies. The FBBN model preserves the core logic of the VIE formulation while enabling probabilistic reasoning and soft evidence integration, thus offering a more robust and transparent tool for risk evaluation. Through the case study of Noirmoutier Island, which encompasses over 21,000 residential buildings, it was demonstrated the model's ability to give probabilistic outputs that not only aligned closely with the original VIE classifications, but also revealed the uncertainty of each vulnerability class. The incorporation of multiple flood scenarios and fuzzy membership functions allowed to consider the progressive nature of vulnerability as flood intensity increases. Sensitivity analysis confirmed the dominant influence of architectural typology and proximity to flood defenses on the overall vulnerability outcome. Moreover, geospatial visualizations provided a powerful means to communicate uncertainty to stakeholders, enabling a better understanding of localized risk patterns. By identifying buildings with high probabilities of extreme vulnerability, local authorities can better allocate resources to retrofitting, emergency planning, or relocation. Its application can be extended to other geographic regions with appropriate recalibration, making it a transferable and scalable solution.

A major challenge in this study was the lack of detailed architectural data, which limits the precision of vulnerability assessments at the micro-scale. However, the Fuzzy-Bayesian framework offers a promising solution by allowing the integration of uncertainty. Future work should leverage regional architectural statistics, such as the high proportion of single-story buildings on Noirmoutier Island, to inform prior probabilities, enabling more comprehensive and less biased vulnerability estimates even when data are incomplete.

Table A.7
Values of the membership functions for the baseline (case study in Fig. 4) and alternative values for the sensitivity analysis (Fig. 9)

Criterion	Category	Baseline			Alternative values		
		a	*b*	*c*	*a*	*b*	*c*
CR1	No Flooded	–	0.45	1.075	–	0.65	1.6
	0 to 0,5 m	0.45	1.075	1.7	0.65	1.6	2.2
	0,5 to 1 m	1.075	1.7	2.45	1.6	2.2	3.2
	1 to 2 m	1.7	2.45	3.2	2.2	3.2	4.2
	2 m or more	2.45	3.2	–	3.2	4.2	–
CR2	Beyond 400 m	–	0.5	1.2	–	0.5	1
	Between h*100 and 400 mm	0.5	1.2	1.9	0.5	1	2
	Between 100 m and h*100 m	1.2	1.9	2.6	1	2	3
	Less than 100 m	1.9	2.6	–	2	3	–
CR3	Ground-floor unoccupied	–	0.5	1.2	–	0.5	1.5
	Two floors	0.5	1.2	1.9	0.5	1.5	2.2
	Single storey with rescue level	1.2	1.9	2.6	1.5	2.2	3.2
	Single storey with evacuation	1.9	2.6	3.3	2.2	3.2	4.2
	Single storey without evacuation	2.6	3.3	–	3.2	4.2	–
CR4	On a natural rescue point (NRP)	–	0.65	1.6	–	0.65	1.6
	Less than 100 m of a NRP	0.65	1.6	2.55	0.65	1.6	2.2
	Between 100 m and 200 m of a NRP	1.6	2.55	3.5	1.6	2.2	3.2
	More than 200 m of a NRP	2.55	3.5	4.45	2.2	3.2	4.2
	More than 200 m of a NRP and isolated	3.5	4.45	–	3.2	4.2	–

In future extensions, the framework is intended to be dynamic, with the ability to incorporate multiple databases and evolve into a dynamic Bayesian network to account for time-varying parameters. This would enable the CPTs to be updated with empirical outcomes as new data becomes available, enhancing the model's ability to infer and adapt to changing conditions. Such advancements would allow the framework to move beyond its current role as an uncertainty wrapper and serve as a more flexible and data-driven tool for vulnerability and risk assessment.

Future research will focus on expanding the applications of our framework to address broader challenges in vulnerability and risk management. The probabilistic nature of the framework offers significant potential to support life-cycle cost analysis, enabling the evaluation of the long-term costs and benefits of various risk mitigation strategies. Additionally, incorporating social vulnerability indicators (such as age, gender, season, and time of day) would allow for a more comprehensive assessment by capturing the diverse ways in which different populations are affected by floods.

Expanding the framework to include adaptation strategies will also enable the evaluation of not only vulnerability but the effectiveness of mitigation measures, while accounting for uncertainty and economic factors. These advancements would support the development of targeted, house-specific mitigation strategies, ensuring more effective and equitable protection of human life during coastal flood events. Furthermore, exploring adaptive planning under uncertainty will enhance decision-making in contexts with ambiguous future scenarios, such as those driven by climate change impacts. Ultimately, these improvements aim to increase the robustness and applicability of the methodology, providing a more holistic approach to comprehensive risk management in flood-prone areas.

CRediT authorship contribution statement

Valentina Velandia-Diaz: Writing – original draft, Visualization, Software, Methodology, Investigation, Formal analysis, Data curation, Conceptualization. **Emilio Bastidas-Arteaga:** Writing – review & editing, Validation, Supervision, Methodology, Investigation, Funding acquisition, Formal analysis, Conceptualization. **Axel Creach:** Writing – review & editing, Investigation, Data curation, Conceptualization. **Solomon Tesfamariam:** Writing – review & editing, Validation, Supervision, Methodology, Investigation, Formal analysis, Conceptualization.

Declaration of competing interest

The authors declare that they have no known competing financial interests or personal relationships that could have appeared to influence the work reported in this paper.

Acknowledgments

This research was funded by l'Agence Nationale de la Recherche (ANR), project ANR-23-CE22-0011, the Research Grants Council (RGC) Joint Research Scheme (A-PolyU502/23), as well as by the European Union, project 101128171 – NORISK – ERASMUS-EDU-2023-PEX-EMJM-MOB. Views and opinions expressed are those of the authors only and do not necessarily reflect those of the funding agencies. Neither the ANR, RGC or the EACEA can be held responsible for them.

Appendix. Values of membership functions

Table A.7 provides the values of the parameters of the membership functions used in this study as well as those used in the analysis of Fig. 9.

Data availability

Data will be made available on request.

References

[1] IPCC, Romero J. IPCC, 2023: Climate Change 2023: Synthesis Report. Contribution of Working Groups I, II and III to the Sixth Assessment Report of the Intergovernmental Panel on Climate Change [Core Writing Team, H. Lee and J. Romero (eds.)]. IPCC, Geneva, Switzerland. Technical Report, Intergovernmental Panel on Climate Change (IPCC); 2023, Edition: First, URL https://www.ipcc.ch/report/ar6/syr/.

[2] IPCC. The Ocean and Cryosphere in a Changing Climate: Special Report of the Intergovernmental Panel on Climate Change. 1st ed.. Cambridge University Press; 2019, URL https://www.cambridge.org/core/product/identifier/9781009157964/type/book.

[3] Tramblay Y, Thirel G, Strohmenger L, Evin G, Corre L, Heraut L, Sauquet E. Evolution of flood generating processes under climate change in France. 2025, http://dx.doi.org/10.5194/egusphere-2025-1635, URL https://egusphere.copernicus.org/preprints/2025/egusphere-2025-1635/.

[4] United Nations International Strategy for Disaster Reduction Secretariat, editor. Making development sustainable: the future of disaster risk management. In: Global assessment report on disaster risk reduction, (2015). Geneva; 2015.

[5] Prashar N, Lakra HS, Shaw R, Kaur H. Urban flood resilience: A comprehensive review of assessment methods, tools, and techniques to manage disaster. Prog Disaster Sci 2023;20:100299, URL https://linkinghub.elsevier.com/retrieve/pii/S2590061723000261.

[6] Wang H-W, Castillo Castro DS, Chen G-W. Managing residual flood risk: Lessons learned from experiences in Taiwan. Prog Disaster Sci 2024;23:100337, URL https://linkinghub.elsevier.com/retrieve/pii/S2590061724000279.

[7] Lumbroso DM, Vinet F. A comparison of the causes, effects and aftermaths of the coastal flooding of England in 1953 and France in 2010. Nat Hazards Earth Syst Sci 2011;11(8):2321–33, URL https://nhess.copernicus.org/articles/11/2321/2011/.

[8] Bertin X, Bruneau N, Breilh J-F, Fortunato AB, Karpytchev M. Importance of wave age and resonance in storm surges: The case Xynthia, bay of Biscay. Ocean Model 2012;42:16–30, URL https://linkinghub.elsevier.com/retrieve/pii/S1463500311001776.

[9] Verger F. Digues et polders littoraux : réflexions après la tempête xynthia. Physio-Géo 2011;(Volume 5):95–105, URL http://journals.openedition.org/physio-geo/1740.

[10] Chauveau E, Chadenas C, Comentale B, Pottier P, Blanlœ il A, Feuillet T, Mercier D, Pourinet L, Rollo N, Tillier I, Trouillet B. Xynthia: lessons learned from a catastrophe. Cybergeo 2017. URL http://journals.openedition.org/cybergeo/28032.

[11] Vinet F, Lumbroso D, Defossez S, Boissier L. A comparative analysis of the loss of life during two recent floods in France: the sea surge caused by the storm xynthia and the flash flood in var. Nat Hazards 2012;61(3):1179–201, URL http://link.springer.com/10.1007/s11069-011-9975-5.

[12] Tikuye BG, Ray RL, Abeysingha NS, Gurau S. Integrating multi-criteria decision analysis and geospatial data for flood susceptibility mapping in texas, USA. Prog Disaster Sci 2025;28:100462, URL https://linkinghub.elsevier.com/retrieve/pii/S2590061725000596.

[13] Mudashiru RB, Sabtu N, Abustan I, Balogun W. Flood hazard mapping methods: A review. J Hydrol 2021;603:126846.

[14] Spachinger K, Dorner W, Metzka R, Serrhini K, Fuchs S. Flood risk and flood hazard maps – visualisation of hydrological risks. IOP Conf Ser: Earth Environ Sci 2008;4:012043, URL https://iopscience.iop.org/article/10.1088/1755-1307/4/1/012043.

[15] Farid M, Sihombing YI, Kuntoro AA, Adityawan MB, Syuhada MM, Januriyadi NF, Moe IR, Nurhakim A. Development of flood hazard index under climate change scenarios in java island. Prog Disaster Sci 2023;20:100302, URL https://linkinghub.elsevier.com/retrieve/pii/S2590061723000297.

[16] Wang J, Yun X, Pokhrel Y, Yamazaki D, Zhao Q, Chen A, Tang Q. Modeling daily floods in the lancang-mekong river basin using an improved hydrological-hydrodynamic model. Water Resour Res 2021;57(8). e2021WR029734. URL https://agupubs.onlinelibrary.wiley.com/doi/10.1029/2021WR029734.

[17] Fahad MGR, Nazari R, Motamedi M, Karimi M. A decision-making framework integrating fluid and solid systems to assess resilience of coastal communities experiencing extreme storm events. Reliab Eng Syst Saf 2022;221:108388.

[18] Lu Y, Zhai G, Zhou S. An integrated Bayesian networks and geographic information system (BNs-GIS) approach for flood disaster risk assessment: A case study of yinchuan, China. Ecol Indic 2024;166:112322, URL https://linkinghub.elsevier.com/retrieve/pii/S1470160X24007799.

[19] Banan-Dallalian M, Shokatian-Beiragh M, Golshani A, Abdi A. Use of a Bayesian network for storm-induced flood risk assessment and effectiveness of ecosystem-based risk reduction measures in coastal areas (port of sur, sultanate of oman). Ocean Eng 2023;270:113662, URL https://linkinghub.elsevier.com/retrieve/pii/S002980182300046X.

[20] Zwirglmaier V, Garschagen M. Linking urban structure types and Bayesian network modelling for an integrated flood risk assessment in data-scarce mega-cities. Urban Clim 2024;56:102034, URL https://linkinghub.elsevier.com/retrieve/pii/S221209552400230X.

[21] Jang S-D, Yoo J-H, Lee Y-S, Kim B. Flood prediction in urban areas based on machine learning considering the statistical characteristics of rainfall. Prog Disaster Sci 2025;26:100415, URL https://linkinghub.elsevier.com/retrieve/pii/S2590061725000122.

[22] Wang Y, Ye Z, Jia X, Liu H, Zhou G, Wang L. Flood disaster chain deduction based on cascading failures in urban critical infrastructure. Reliab Eng Syst Saf 2025;261:111160.

[23] Kaur M, Sultana S, Ishaq S, Saleem S, Nahiduzzaman KM, Hewage K, Sadiq R. Building a flood vulnerability index for urban resilience: Insights from kelowna, british columbia. J Urban Manag 2025. S2226585625000457. URL https://linkinghub.elsevier.com/retrieve/pii/S2226585625000457.

[24] Borden KA, Schmidtlein MC, Emrich CT, Piegorsch WW, Cutter SL. Vulnerability of U.S. cities to environmental hazards. J Homel Secur Emerg Manag 2007;4(2). URL https://www.degruyter.com/document/doi/10.2202/1547-7355.1279/html.

[25] Blaikie PM, editor. At risk: natural hazards, people's vulnerability, and disasters. London ; New York: Routledge; 1994.

[26] Wu Z, Shen Y, Wang H, Wu M. Assessing urban flood disaster risk using Bayesian network model and GIS applications. Geomatics, Nat Hazards Risk 2019;10(1):2163–84, URL https://www.tandfonline.com/doi/full/10.1080/19475705.2019.1685010.

[27] Ţîncu R, Zêzere JL, Crăciun I, Lazăr G, Lazăr I. Quantitative micro-scale flood risk assessment in a section of the trotuş river, Romania. Land Use Policy 2020;95:103881, URL https://linkinghub.elsevier.com/retrieve/pii/S0264837718311116.

[28] Rehan BM. An innovative micro-scale approach for vulnerability and flood risk assessment with the application to property-level protection adoptions. Nat Hazards 2018;91(3):1039–57, URL http://link.springer.com/10.1007/s11069-018-3175-5.

[29] Ernst J, Dewals BJ, Detrembleur S, Archambeau P, Erpicum S, Pirotton M. Micro-scale flood risk analysis based on detailed 2D hydraulic modelling and high resolution geographic data. Nat Hazards 2010;55(2):181–209, URL http://link.springer.com/10.1007/s11069-010-9520-y.

[30] De Risi R, Jalayer F, Iervolino I, Manfredi G, Carozza S, et al. VISK: a GIS-compatible platform for micro-scale assessment of flooding risk in urban areas. In: COMPDYN, 4th ECCOMAS thematic conference on computational methods in structural dynamics and earthquake engineering. kos island, Greece. 2013.

[31] Brazdova M, Riha J. A simple model for the estimation of the number of fatalities due to floods in central europe. Nat Hazards Earth Syst Sci 2014;14(7):1663–76.

[32] Jonkman SN, Kelman I. An analysis of the causes and circumstances of flood disaster deaths. Disasters 2005;29(1):75–97.

[33] Antoni V, Joassard I. Chiffres clés des risques naturels - édition 2023. 2024, URL https://www.statistiques.developpement-durable.gouv.fr/chiffres-cles-des-risques-naturels-edition-2023. [Accessed 18 June 2025].

[34] Diermanse F, Geerse C. Correlation models in flood risk analysis. Reliab Eng Syst Saf 2012;105:64–72.

[35] Creach A, Pardo S, Guillotreau P, Mercier D. The use of a micro-scale index to identify potential death risk areas due to coastal flood surges: lessons from storm xynthia on the french atlantic coast. Nat Hazards 2015;77(3):1679–710, URL http://link.springer.com/10.1007/s11069-015-1669-y.

[36] Creach A, Bastidas-Arteaga E, Pardo S, Mercier D. Chapter eight - adaptation of residential buildings to coastal floods: Strategies, costs and efficiency. In: Bastidas-Arteaga E, Stewart MG, editors. Climate adaptation engineering. Butterworth-Heinemann; 2019, p. 245–70, URL https://www.sciencedirect.com/science/article/pii/B9780128167823000085.

[37] Creach A, Bastidas-Arteaga E, Pardo S, Mercier D. Vulnerability and costs of adaptation strategies for housing subjected to flood risks: Application to la guérinière France. Mar Policy 2020;117:103438, URL https://linkinghub.elsevier.com/retrieve/pii/S0308597X16306303.

[38] Cockburn G, Tesfamariam S. Earthquake disaster risk index for Canadian cities using Bayesian belief networks. Georisk: Assess Manag Risk Eng Syst Geohazards 2012;6(2):128–40, URL http://www.tandfonline.com/doi/abs/10.1080/17499518.2011.650147.

[39] Tesfamariam S, Martín-Pérez B. Bayesian belief network to assess carbonation-induced corrosion in reinforced concrete. J Mater Civ Eng 2008;20(11):707–17.

[40] Abebe Y, Kabir G, Tesfamariam S. Assessing urban areas vulnerability to pluvial flooding using GIS applications and Bayesian belief network model. J Clean Prod 2018;174:1629–41, URL https://linkinghub.elsevier.com/retrieve/pii/S0959652617327245.

[41] Tran T-B, Bastidas-Arteaga E. Spatial variability identification of carbonation depth in concrete using Bayesian networks. Struct Saf 2025;117:102632.

[42] Shahriar A, Sadiq R, Tesfamariam S. Risk analysis for oil & gas pipelines: A sustainability assessment approach using fuzzy based bow-tie analysis. J Loss Prev Process Ind 2012;25(3):505–23, URL https://linkinghub.elsevier.com/retrieve/pii/S0950423011002154.

[43] Tesfamaraim S, Saatcioglu M. Seismic risk assessment of RC buildings using fuzzy synthetic evaluation. J Earthq Eng 2008;12(7):1157–84, URL https://www.tandfonline.com/doi/full/10.1080/13632460802003785.

[44] Ahmad SS, Simonovic SP. Spatial and temporal analysis of urban flood risk assessment. Urban Water J 2013;10(1):26–49, URL http://www.tandfonline.com/doi/abs/10.1080/1573062X.2012.690437.

[45] Creach A. Cartographie et analyse économique de la vulnérabilité du littoral atlantique français face au risque de submersion marine (Ph.D. thesis), Université de Nantes; 2015, NNT: tel-01275600. URL https://theses.hal.science/tel-01275600.

[46] IGNand SHOM. Litto3D v1.0: Spécifications techniques. Technical Report, IGN and SHOM; 2012, URL https://services.data.shom.fr/static/specifications/DC_Litto3D.pdf.

[47] Ministère de l'Ecologie, du Développement Durable, des Transports et du Logement. Circulaire du 27 juillet 2011 relative à la prise en compte du risque de submersion marine dans les plans de prévention des risques naturels littoraux. 2011, MEDDTL no 2011/15 du 25 août 2011, pp 87-103, https://www.bulletin-officiel.developpement-durable.gouv.fr.

[48] European Parliament and Council. Directive 2007/60/EC of the European parliament and of the council of 23 october 2007 on the assessment and management of flood risks (text with EEA relevance). 2007, OJ L 288, 6.11.2007, pp. 27–34, https://eur-lex.europa.eu/legal-content/EN/TXT/?uri=celex:32007L0060.

[49] DREAL Pays de la Loire. Rapport de présentation de la cartographie du risque de submersion marine sur le secteur Noirmoutier-Saint Jean de Monts (Directive inondations Bassins Loire-Bretagne). Technical Report, DREAL Pays de la Loire; 2014.

[50] Zadeh L. Fuzzy sets. Inf Control 1965;8(3):338–53, URL https://linkinghub.elsevier.com/retrieve/pii/S001999586590241X.

[51] Tesfamariam S, Saatcioglu M. Seismic risk assessment of reinforced concrete buildings using fuzzy rule based modeling. In: Proceedings of the 14th world conference on earthquake engineering. Beijing, China: International Association for Earthquake Engineering; 2008, Paper No. 09-01-0167.

[52] González P, Idais H, Pasadas M, Yasin M. Approximation of fuzzy functions by fuzzy interpolating bicubic splines: 2018 CMMSE conference. J Math Chem 2019;57(5):1252–67, URL http://link.springer.com/10.1007/s10910-018-0946-x.

[53] Pearl J. Probabilistic Reasoning in Intelligent Systems: Networks of Plausible Inference. Elsevier Reference Monographs; 1988, 1. aufl, s.l..

[54] Cai W, Zhu X, Peng A, Wang X, Fan Z. Flood risk analysis for cascade dam systems: A case study in the dadu river basin in China. Water 2019;11(7):1365, URL https://www.mdpi.com/2073-4441/11/7/1365.

[55] Sjökvist S, Hansson F. Modelling expert judgement into a Bayesian belief network: A method for consistent and robust determination of conditional probability tables. Lund University; 2013.

[56] Feng X, Williams CKI. Training Bayesian networks for image segmentation. Math Model Estim Tech Comput Vis 1998;3457.

[57] Jung M-K, Kim J-Y, Kwon H, Lee B-S. Exploring the combined risk of sea level rise and storm surges using a Bayesian network model: Application to saemangeum seawall. J Coast Res 2021;114:186–90.

[58] Laskey K. Sensitivity analysis for probability assessments in Bayesian networks. IEEE Trans Syst Man Cybern 1995;25(6):901–9.

[59] Pearl J. Probabilistic reasoning in intelligent systems: networks of plausible inference. Elsevier; 2014.

[60] Fattal P, Robin M, Paillart M, Maanan M, Mercier D, Lamberts C, Costa S. Effects of storms on a developed beach with strong coastal protection: éloux beach (noirmoutier coast, vendée, France). Norois 2010;(215):101–14.

[61] Creach A. VIE (extreme intrinsic vulnerability) index database | données indice VIE (vulnérabilité intrinsèque extrême). 2024, https://doi.org/10.35110/ba5fbe44-4643-4bd6-b191-765d89bde1a6.

[62] INSEE. Recensement général de la population 2011. 2014, Publié le 26 juin 2014, http://www.insee.fr/fr/bases-de-donnees/default.asp?page=recensements.htm.